

Effects of center-of-mass correction and nucleon anomalous magnetic moments on nuclear charge radii

Yusuke Tanimura^{1,2} and Myung-Ki Cheoun¹

¹*Department of Physics and Origin of Matter and Evolution of Galaxies (OMEG) Institute, Soongsil University, Seoul 06978, Korea*
²*Department of Physics, Tohoku University, Sendai, 980-8578, Japan*

(Dated: December 27, 2023)

Effects of the center-of-mass (CM) correction together with the nucleon electromagnetic form factors on the nuclear charge radius are systematically studied with a relativistic Hartree-Bogoliubov model. Both one- and two-body parts of the CM correction are taken into account. It is found that the one- and two-body CM corrections, and the spin-orbit effect originating from the nucleon anomalous magnetic moments are all of the same order in magnitude, and that they give sizable impacts on the charge radius from light to heavy nuclei.

I. INTRODUCTION

The nuclear charge radius is one of the most fundamental observables of the atomic nucleus, which is measured accurately by the electromagnetic probes such as electron scattering and atomic laser spectroscopy [1–13]. Although the charge radius represents simply the size of the nuclear many-body system, it exhibits signals of the nuclear structure effects such as the shell effect [11, 12, 15–17], pairing correlation [7, 9–11, 18], and deformation [6, 13, 14, 19]. The quantum fluctuation of the nuclear shape can also have considerable effects on the charge radius [20, 21]. It is also argued that the difference of charge radii between a pair of mirror nuclei is correlated with the nuclear symmetry energy [5, 9, 22–26]. Therefore, the precise theoretical interpretation of the charge radius is intimately related to various many-body and electromagnetic effects as well as the understanding of nuclear force.

Among the nuclear many-body theory, the mean-field model [27–31] is suitable to study the systematic behaviors of the charge radius. It describes the nuclear many-body system in a microscopic manner with a universal energy density functional (EDF). Properties of the atomic nucleus such as binding energy, size, and electromagnetic moments are the basic ground-state observables that one wishes to describe with the model. An essential feature of the mean-field model is the breaking of the symmetries possessed by the many-body Hamiltonian. On the one hand, it introduces additional correlations within a single product-state wave function, and on the other hand, it necessitates restoration of symmetries or correction of the observables for the symmetry breaking [28–31].

The translational invariance is always violated in the mean-field model for finite nuclei since a many-body state is constructed as nucleons bound in a mean-field potential which is fixed in space. The center of mass (CM) of the state is localized around the potential and gives spurious contributions to observables. In principle, one should restore the symmetry by a projection method, [28–32], which is numerically costly for realistic calculations. In most applications, the spurious effect is ei-

ther neglected or removed in various approximate ways from the binding energy and the charge radius [33–40]. Recently, the CM correction on the binding energy was extensively discussed in Ref. [34] with a particular focus on the impact of the two-body operator part of the CM kinetic energy, which has been neglected in many of the existing EDFs. The significant effects of the two-body part on the surface-energy coefficient and the deformation energy were demonstrated [33, 34].

In this work, we assess the correction of the charge radius for the violation of translational invariance. The correction is made by removing the effect of the zeropoint fluctuation of the CM in calculating the expectation value of the squared radius. As in the case of the CM kinetic energy [33, 34], there arise one- and two-body parts of the correction of the expectation value. The CM correction of the radius has often been completely neglected, although it is taken into account in some of the existing functionals with the one- and two-body parts [35, 36] in an approximate way [37], with only the one-body part [36, 38]. Note that, for the charge radius, the CM correction can also be taken into account in the nuclear charge form factors by an approximate projection technique [32, 41] (see also Refs. [28, 29, 42–44]). The connection between our approach and the projection method will also be discussed via a harmonic-oscillator model.

In addition to the CM correction, it is important also to consider the electromagnetic structure of the nucleon for precise description of the charge radius, which is reflected in the electromagnetic form factors. Notice that the form factors of nucleon directly affect the nuclear charge-density distribution. In particular, the effect of the so-called “spin-orbit” contribution due to the anomalous magnetic moment of nucleon is sensitive to the shell structure, as has long been discussed [41, 42, 45–49]. Since it is an $O((v/c)^2)$ effect, it would be comparable to the CM correction of $O(1/A)$.

Therefore, in the present work, we take into account the full CM correction of the charge radius, including its two-body part, together with the nucleon electromagnetic form factors to study systematically i) the contributions to the charge radius from CM correction and

anomalous magnetic coupling, and ii) the impact of the corrections on the charge radius, in comparison with the experimental data. To be consistent with the electromagnetism formulated in a covariant way, it is appropriate to treat the nuclear many-body system with a relativistic theory. For this purpose, therefore, we employ a relativistic Hartree-Bogoliubov (RHB) model. It should also be noted that the significance of the relativistic nuclear mean fields in the anomalous magnetic coupling term has been pointed out in Refs. [46, 50].

The paper is organized as follows. In Sec. II, we describe how the CM correction and anomalous magnetic coupling effect modify the calculation of charge radius. The analysis of the corrections and comparison with experimental data are presented in Sec. III. Lastly, summary and outlook is given in Sec. IV.

II. MODEL

A. Relativistic Hartree-Bogoliubov model

We employ an RHB model with DDME2 parameter set [51] for the ph channel and Gogny D1S interaction [52, 53] for the pp channel. A remark on DDME2 is in order: the parameter fit to charge radii was made by $r_{\text{ch}} = \sqrt{\langle r^2 \rangle_p + (0.8 \text{ fm})^2}$, where $\langle r^2 \rangle_p$ is the mean-squared (MS) radius of point-proton density distribution, and $(0.8 \text{ fm})^2$ is a correction for the charge radius of the proton itself, with BCS calculations instead of Hartree-Bogoliubov. The CM correction and anomalous magnetic coupling described in the following subsections were not considered. See Refs. [51, 54–60] for details of the RHB model and the DDME2 parameter set. We impose the spherical symmetry and solve the RHB equations in the radial coordinate space.

B. Center-of-mass correction on mean-squared radii

The mean-square (MS) radius $\langle r^2 \rangle_p$ of proton distribution, without CM correction, is given as

$$Z \langle r^2 \rangle_p = \left\langle \sum_{i \in p} \mathbf{r}_i^2 \right\rangle = \int d^3r r^2 \rho_p(\mathbf{r}), \quad (1)$$

where \mathbf{r}_i is the position of the i th proton. The correction for the spurious CM contribution should be made by

$$\begin{aligned} Z \langle r^2 \rangle_{p,\text{corr}} &= \left\langle \sum_{i \in p} (\mathbf{r}_i - \mathbf{R}_G)^2 \right\rangle \\ &\equiv Z \left[\langle r^2 \rangle_p + \Delta_p^{(\text{CM1})} + \Delta_p^{(\text{CM2})} \right], \quad (2) \end{aligned}$$

where $\mathbf{R}_G = (1/A) \sum_{i=1}^A \mathbf{r}_i$ is the CM position of the nucleus, and the one- and two-body parts of the cor-

rection, $\Delta_p^{(\text{CM}i)}$ ($i = 1, 2$), are given by

$$\Delta_p^{(\text{CM1})} = -\frac{2}{AZ} \sum_{\alpha \in p} v_\alpha^2 \langle \alpha | r^2 | \alpha \rangle + \frac{1}{A^2} \sum_{\alpha} v_\alpha^2 \langle \alpha | r^2 | \alpha \rangle, \quad (3)$$

$$\begin{aligned} \Delta_p^{(\text{CM2})} &= +\frac{2}{AZ} \sum_{\alpha\beta \in p} (v_\alpha^2 v_\beta^2 - u_\alpha v_\alpha u_\beta v_\beta) |\langle \alpha | \mathbf{r} | \beta \rangle|^2 \\ &\quad - \frac{1}{A^2} \sum_{\alpha\beta} (v_\alpha^2 v_\beta^2 - u_\alpha v_\alpha u_\beta v_\beta) |\langle \alpha | \mathbf{r} | \beta \rangle|^2, \quad (4) \end{aligned}$$

respectively. u_α and v_α are the occupation amplitudes of the canonical single-particle state α [30]. Notice that the summation of the first terms in Eqs. (3) and (4) runs over the proton states only whereas the one in the second terms runs over both the proton and the neutron states. See Appendix A for a derivation of Eqs. (3) and (4).

C. Effect of anomalous magnetic moment and finite size of nucleon

In general, the nuclear charge form factor is given by [41, 46, 50, 61, 65]

$$\begin{aligned} \tilde{\rho}_{\text{ch}}(\mathbf{q}) &= \sum_{\tau=p,n} \int d^3r e^{i\mathbf{q}\cdot\mathbf{r}} [F_{1\tau}(q^2) \rho_\tau(\mathbf{r}) \\ &\quad + F_{2\tau}(q^2) \rho_{\kappa\tau}(\mathbf{r})], \quad (5) \end{aligned}$$

where in the mean-field approximation

$$\rho_\tau(\mathbf{r}) = \sum_{\alpha \in \tau} v_\alpha^2 \psi_\alpha^\dagger(\mathbf{r}) \psi_\alpha(\mathbf{r}), \quad (6)$$

$$\rho_{\kappa\tau}(\mathbf{r}) = \kappa_\tau \frac{\hbar}{2mc} \nabla \cdot \sum_{\alpha \in \tau} v_\alpha^2 \bar{\psi}_\alpha(\mathbf{r}) i \boldsymbol{\alpha} \psi_\alpha(\mathbf{r}), \quad (7)$$

with ψ_α being the wave function of a canonical single-particle state α . In Eq. (7), m is the nucleon mass, $\kappa_p = 1.793$ and $\kappa_n = -1.913$ are the anomalous magnetic moments of nucleon, and $\boldsymbol{\alpha} = \gamma^0 \boldsymbol{\gamma}$ is the usual Dirac matrix. The nucleon form factors $F_1(q^2)$ and $F_2(q^2)$ contain the information about the internal electromagnetic structure of nucleon. Note that their values at zero momentum transfer are identified as $F_1(0) = Q$ and $2[F_1(0) + \kappa F_2(0)] = g$, where Q is the electric charge, and g is the g factor of nucleon [66]. Thus they are normalized as $F_{1p}(0) = F_{2p}(0) = F_{2n}(0) = 1$, and $F_{1n}(0) = 0$.

The nuclear MS charge radius without the CM correction, which we denote here as $\langle r^2 \rangle'_{\text{ch}}$, is given by

$$\begin{aligned} \langle r^2 \rangle'_{\text{ch}} &= -\frac{\nabla^2 \tilde{\rho}_{\text{ch}}(\mathbf{q})|_{\mathbf{q}=0}}{\tilde{\rho}_{\text{ch}}(\mathbf{0})} \\ &= \langle r^2 \rangle_p + \langle r^2 \rangle_\kappa + C_p + \frac{N}{Z} C_n, \quad (8) \end{aligned}$$

where

$$\langle r^2 \rangle_\kappa = \frac{1}{Z} \sum_{\tau=p,n} \int d^3r r^2 \rho_{\kappa\tau}(\mathbf{r}), \quad (9)$$

and C_τ ($\tau = p, n$) are the constants independent of the nuclear structure,

$$\begin{aligned} C_\tau &= -6 \left. \frac{dF_{1\tau}}{dq^2} \right|_{q^2=0} \\ &= -6 \left. \frac{dG_{E\tau}}{dq^2} \right|_{q^2=0} - \frac{3\hbar^2}{2m^2c^2} \kappa_\tau. \end{aligned} \quad (10)$$

Here, $G_{E\tau} = F_{1\tau} - q^2 (\hbar/2mc)^2 \kappa_\tau F_{2\tau}$ is the electric Sachs form factor [62–65, 67]. The first term in Eq. (10) is interpreted as the MS charge radius of the nucleon itself [64, 68, 69]. We take the experimental values [70] for proton and neutron charge radii,

$$-6 \left. \frac{dG_{Ep}}{dq^2} \right|_{q^2=0} = (0.841 \text{ fm})^2, \quad (11)$$

$$-6 \left. \frac{dG_{En}}{dq^2} \right|_{q^2=0} = -0.116 \text{ fm}^2. \quad (12)$$

Therefore, for given densities ρ_p and $\rho_{\kappa\tau}$ of point nucleons, the momentum dependence of the form factors, or the finite-size effect, only adds a constant to the MS radius of point-nucleon charge distribution.

In this work, we calculate the charge radius in the following way. In the RHB calculations, we take $F_{1\tau}(q^2) = F_{1\tau}(0)$ and $F_{2\tau}(q^2) = F_{2\tau}(0)$, i.e., we take into account the effect of the point-nucleon anomalous magnetic moment. The charge density is then given as

$$\rho_{\text{ch}}(\mathbf{r}) = \rho_p(\mathbf{r}) + \sum_{\tau=p,n} \rho_{\kappa\tau}(\mathbf{r}). \quad (13)$$

The first term ρ_p is the point-proton density distribution while the second term ρ_κ describes the contributions of the anomalous magnetic couplings to the charge density. We refer to the latter as the “spin-orbit” term. Since we use momentum-independent form factors, the finite-size effect is still neglected. Instead, the finite size of nucleon will be considered only at the final step to compute the MS charge radius by folding the resulting RHB charge density by the nucleon form factors, and consequently we add simply the C_τ terms to the MS radius. We expect this is enough to the first approximation since the finite-size effect would give nearly the constant shift to the MS charge radius unless the complicated many-body effects [28] on the nucleon form factors are explicitly considered. Note also that, according to the extra term $\sum_\tau \rho_{\kappa\tau}$ of the charge density in Eq. (13), the equations of motion to be solved in the mean-field calculation for the electrostatic and the nucleon fields are modified.

With the CM correction on $\langle r^2 \rangle_p$, we have for the MS

charge radius,

$$\begin{aligned} \langle r^2 \rangle_{\text{ch}} &= \langle r^2 \rangle_{p,\text{corr}} + \langle r^2 \rangle_\kappa + C_p + \frac{N}{Z} C_n \\ &= \langle r^2 \rangle_p + \Delta_p^{(\text{CM1})} + \Delta_p^{(\text{CM2})} + \langle r^2 \rangle_\kappa \\ &\quad + \left(0.588 + 0.011 \frac{N}{Z} \text{ fm}^2 \right), \end{aligned} \quad (14)$$

where we have substituted the numerical values for nucleon charge radii [Eqs. (11) and (12)], and the $3\hbar^2\kappa/2m^2c^2$ terms. The first term of Eq. (14) is the MS radius of point proton, the second and third terms are the CM correction of the first, the fourth term is the contribution from the magnetic spin-orbit term, and the last term is the finite-size effect of nucleon introduced by the momentum-dependence of the form factors. Notice that the last term which is independent of the many-body wave function is almost constant with a weak N/Z dependence. In the present work, the CM correction of the small spin-orbit contribution $\langle r^2 \rangle_\kappa$ is neglected. The root-mean-square (RMS) charge radius is defined as

$$r_{\text{ch}} = \sqrt{\langle r^2 \rangle_{\text{ch}}}. \quad (15)$$

III. RESULTS AND DISCUSSIONS

With the model described in the previous section, we calculate the charge radii of even-even nuclei in the isotope chains $^4\text{-}^8\text{He}$, $^{10}\text{-}^{22}\text{C}$, $^{12}\text{-}^{28}\text{O}$, $^{36}\text{-}^{56}\text{Ca}$, $^{50}\text{-}^{80}\text{Ni}$, $^{78}\text{-}^{112}\text{Zr}$, $^{100}\text{-}^{148}\text{Sn}$, and $^{180}\text{-}^{220}\text{Pb}$.

For brevity, the one- and two-body CM correction, $\Delta_p^{(\text{CM1})}$ and $\Delta_p^{(\text{CM2})}$, and the spin-orbit term $\langle r^2 \rangle_\kappa$ will be referred to as CM1, CM2, and SO, respectively.

A. Contribution of each correction

Before making a direct comparison of calculated and measured values of the charge radius, we first show in Fig. 1 the contributions to the MS charge radius of the three terms, the SO term, $\langle r^2 \rangle_\kappa$, with magenta triangles, the CM1 term, $\Delta_p^{(\text{CM1})}$, with skyblue squares, and the CM2 term, $\Delta_p^{(\text{CM2})}$, with purple squares. The sum of the three is shown by black dots. The gray bands in the figure show, as a reference to the size of experimental uncertainty, the range given by $\Delta\langle r^2 \rangle(\text{exp}) \in [(r_{\text{ch}} - \delta r_{\text{ch}})^2 - r_{\text{ch}}^2 : (r_{\text{ch}} + \delta r_{\text{ch}})^2 - r_{\text{ch}}^2]$, with r_{ch} and δr_{ch} being the measured value of the charge radius and the associated error, respectively.

Remarkably, all of the three correction terms are of the same order of magnitude, and furthermore, each contribution as well as their sum are much larger than the size of experimental uncertainty except for a few cases. It implies that the three contributions have to be considered if one strives for precise description of the nuclear charge radius.

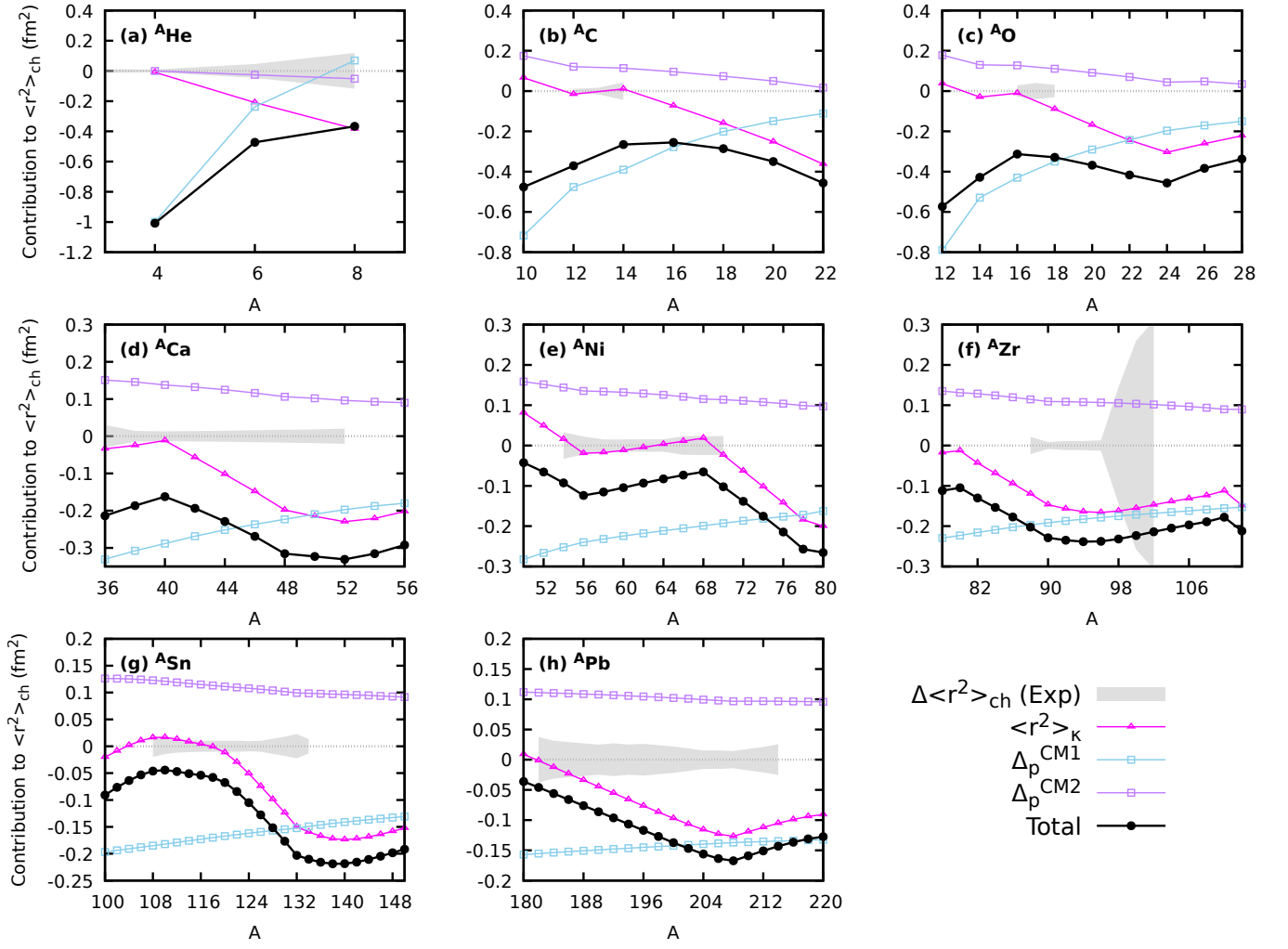


FIG. 1. Contributions of each correction term to the MS charge radius for (a) He, (b) C, (c) O, (d) Ca, (e) Ni, (f) Zr, (g) Sn, and (h) Pb isotopes. The magenta triangles show the anomalous magnetic contribution $\langle r^2 \rangle_{\kappa}$, the skyblue and purple squares the one- and two-body CM corrections, $\Delta_p^{(\text{CM1})}$ and $\Delta_p^{(\text{CM2})}$, respectively, and black dots the total correction $\langle r^2 \rangle_{\kappa} + \Delta_p^{(\text{CM1})} + \Delta_p^{(\text{CM2})}$. The gray bands show the size of experimental uncertainty $\Delta \langle r^2 \rangle_{\text{ch}} \in [(r_{\text{ch}} - \delta r_{\text{ch}})^2 - r_{\text{ch}}^2 : (r_{\text{ch}} + \delta r_{\text{ch}})^2 - r_{\text{ch}}^2]$, with r_{ch} and δr_{ch} being the measured value of the charge radius and the associated error, respectively. The data for $^{54,56}\text{Ni}$ are taken from Ref. [3], $^{58-70}\text{Ni}$ from Ref. [4], and the others from Refs. [1, 2].

1. Center-of-mass correction

The CM1 and CM2 terms are respectively negative and positive in most cases and rather smooth as functions of the mass number. Since CM1 and CM2 are $O(1/A)$ corrections, their values tend to be more substantial for the light nuclei but smaller and almost constant for heavy nuclei. Moreover, the CM2 term tend to cancel the CM1 term for heavier systems, representing the correct asymptotic behavior of the CM correction for $A \rightarrow \infty$, or infinite-matter limit. Therefore, the CM2 term should not be neglected in particular for heavier nuclei.

An approximation with a harmonic-oscillator model described in Appendix B is helpful to discuss the CM correction. As shown in Appendix B, the harmonic-oscillator model reproduces accurately the RHB results for Ca and heavier nuclei but only qualitatively for the lighter nuclei. With a further crude approximation in the harmonic-oscillator model, $N = Z = A/2$, one finds for the two-body to one-body ratio of the CM correction that

$$\frac{\Delta_p^{(\text{CM2})}}{\Delta_p^{(\text{CM1})}} = -\frac{\bar{N}}{\bar{N} + 2}, \quad (16)$$

where \bar{N} is the harmonic-oscillator quantum number of the highest-occupied major shell. One immediately sees that

the ratio tends to zero for s -shell nuclei and decreases with A towards the asymptotic value -1 for $A \rightarrow \infty$. One observes the similar trend in Fig. 1.

Now let us pick up the He isotopes showing somewhat irregular behavior, for which the harmonic-oscillator model may not work well because of the small mass numbers and the weakly-bound nucleons. As can be seen in Fig. 1(a), $\Delta_p^{(\text{CM1})}$ for ${}^8\text{He}$ becomes positive, and $\Delta_p^{(\text{CM2})}$ is negative for ${}^6\text{He}$ and ${}^8\text{He}$. From Eq. (3), we have for the CM1 correction,

$$\Delta_p^{(\text{CM1})} = \frac{1}{A} \left[-2 \left(1 - \frac{Z}{2A} \right) \langle r^2 \rangle_p + \frac{N}{A} \langle r^2 \rangle_n \right] = \begin{cases} \frac{1}{8} \left(-3 \langle r^2 \rangle_p + \langle r^2 \rangle_n \right) & \text{for } {}^4\text{He}, \\ \frac{1}{18} \left(-5 \langle r^2 \rangle_p + 2 \langle r^2 \rangle_n \right) & \text{for } {}^6\text{He}, \\ \frac{1}{32} \left(-7 \langle r^2 \rangle_p + 3 \langle r^2 \rangle_n \right) & \text{for } {}^8\text{He}, \end{cases} \quad (17)$$

where $\langle r^2 \rangle_n$ is the MS radius of neutron. Thus it is determined by the balance between negative and positive contributions from protons and neutrons, respectively. In the neutron-rich He isotopes, the neutron MS radius enhanced by the weakly-bound p -shell neutrons increases the CM1 term. See Table I for the neutron and proton MS radii and the resulting CM1 term of the He isotopes obtained by the RHB calculations. We note that the similar mechanism applies also to general near-dripline nuclei and that this effect is missing in the harmonic-oscillator model. (See also Fig. 5 in Appendix B for the comparisons of the CM correction between the RHB and the harmonic-oscillator models.) The negative values of the CM2 correction in ${}^6\text{He}$ and ${}^8\text{He}$ can be understood more simply. Since the two protons fill only the s shell, the first term in Eq. (4), which is positive, vanishes for the He isotopes. If we assume roughly that $v_{n1s_{1/2}}^2 \approx 1$ and $v_{n1p_{3/2}}^2 \approx (N-2)/4$ for the occupation probabilities of the neutron $1s_{1/2}$ and $1p_{3/2}$ states, respectively,

$$\Delta_p^{(\text{CM2})} \approx -\frac{2}{3} \frac{N-2}{A^2} I_{sp}^2, \quad I_{sp} \equiv \int dr r G_{n1s_{1/2}}(r) G_{n1p_{3/2}}(r), \quad (18)$$

where $G_{n1s_{1/2}}(r)$ and $G_{n1p_{3/2}}(r)$ are the radial wave functions of the upper component of the canonical neutron $1s_{1/2}$ and $1p_{3/2}$ states, respectively. Since $I_{sp}^2 \sim 1 \text{ fm}^2$, Eq. (18) explains the small negative values of the CM2 term in ${}^6\text{He}$ and ${}^8\text{He}$.

We also mention here the connection of our approach to the approximate projection method [32] via harmonic-oscillator approximation. Within the harmonic-oscillator model as described in Appendix B, the total CM correction given by Eqs. (2)-(4) satisfies

$$\Delta_p^{(\text{CM1})} + \Delta_p^{(\text{CM2})} = -\frac{9\hbar^2}{4\langle \mathbf{P}_{\text{CM}}^2 \rangle}, \quad (19)$$

where \mathbf{P}_{CM} is the CM momentum. On the other hand, it was shown in Ref. [32] that the second-order Gaussian-overlap approximation to the momentum projection yields an effect identical to that with a harmonic-oscillator approximation. In their approximation, the nuclear charge form factor is corrected by an additional factor of $\exp\left(\frac{3\hbar^2 \mathbf{q}^2}{8\langle \mathbf{P}_{\text{CM}}^2 \rangle}\right)$ [32, 41], which coincides with the CM correction of $-\frac{9\hbar^2}{4\langle \mathbf{P}_{\text{CM}}^2 \rangle}$ in Eq. (19). Thus our approach yields, for heavy nuclei, approximately the same correction as the projection method, but not for light or weakly-bound nuclei for which the harmonic-oscillator model is not a good approximation (see Appendix B).

Nucleus	$\langle r^2 \rangle_n$	$\langle r^2 \rangle_p$	$\Delta_p^{(\text{CM1})}$
${}^4\text{He}$	3.91	3.97	-0.999
${}^6\text{He}$	7.54	3.87	-0.237
${}^8\text{He}$	9.84	3.90	0.0688

TABLE I. The neutron and proton MS radii, and the CM1 correction in the unit of fm^2 for He isotopes obtained with the RHB model.

2. Spin-orbit effect

The SO effect is more sensitive than the CM corrections to the shell structure. As a result, the shape of the total correction for the heavier isotopes is determined almost by the SO effect with a shift by the CM correction.

The behavior of $\langle r^2 \rangle_\kappa$ can be qualitatively understood

by a nonrelativistic approximation¹ [41, 47, 49],

$$\rho_\kappa = \frac{\kappa\hbar}{2mc} \nabla \cdot \langle \bar{\psi} i \boldsymbol{\alpha} \psi \rangle \sim -\frac{\kappa\hbar}{2mc} \frac{\hbar}{mc} \nabla \cdot \mathbf{J}, \quad (20)$$

where \mathbf{J} is the nonrelativistic spin-orbit density [72]. By integrating Eq. (20) with r^2 , one finds that

$$Z \langle r^2 \rangle_\kappa \sim \kappa \left(\frac{\hbar}{mc} \right)^2 \sum_a v_a^2 (2j_a + 1) \langle \mathbf{l} \cdot \boldsymbol{\sigma} \rangle_a \quad (21)$$

where a labels a j shell, and v_a^2 and j_a are the occupation probability and the angular momentum of the level a , respectively. The symbol $\langle \mathbf{l} \cdot \boldsymbol{\sigma} \rangle_a$ is defined as

$$\langle \mathbf{l} \cdot \boldsymbol{\sigma} \rangle_a = \begin{cases} +l_a & \text{for } j_a = l_a + 1/2, \\ -l_a - 1 & \text{for } j_a = l_a - 1/2, \end{cases} \quad (22)$$

where l_a is the orbital angular momentum of the level a . Thus neutrons in a $j_> = l + 1/2$ ($j_< = l - 1/2$) shell give negative (positive) contribution to $\langle r^2 \rangle_\kappa$, and a pair of spin-orbit doublet orbitals cancel each other at an LS -closed configuration. Since κ_p is similar in the absolute value to κ_n with the opposite sign, protons make the opposite contribution to $\langle r^2 \rangle_\kappa$ in LS -open nuclei. Thus $\langle r^2 \rangle_\kappa$ approximately vanishes for, e.g., doubly LS -closed or $N = Z$ nuclei. We illustrate here the five isotope chains for which we will show the isotope shifts in the next subsection. In the Ca isotopes shown in Fig. 1(d), the increase towards zero of $\langle r^2 \rangle_\kappa$ up to $N = 20$ and the decrease beyond is understood by the effects of neutrons filling $1d_{3/2}$ and $1f_{7/2}$ shells, respectively. In the Ni isotopes shown in Fig. 1(e), $\langle r^2 \rangle_\kappa \approx 0$ at $N = Z = 28$ due to the approximate isovector character of the SO effect. Above $N = 28$, the neutrons are scattered over the $1p_{3/2}$, $1p_{1/2}$, and $1f_{5/2}$ states by the pairing interaction, which smoothen the variation of $\langle r^2 \rangle_\kappa$. The net increase of $\langle r^2 \rangle_\kappa$ from $N = 28$ to 40 is caused by the $1f_{5/2}$ neutrons. The large negative slope for $N > 40$ is the effect of the $1g_{9/2}$ neutrons. In the Zr isotopes shown in Fig. 1(f), $\langle r^2 \rangle_\kappa \approx 0$ at the doubly LS -closed ^{80}Zr nucleus and decreases as the neutrons are added in the $1g_{9/2}$ shell. In the Sn isotopes shown in Fig. 1(g), although the shell effect on $\langle r^2 \rangle_\kappa$ is smoothened by the pairing correlation, its decrease between $A \approx 120$ and 132 is caused mainly by the $1h_{11/2}$ neutrons. Finally, in the Pb isotopes shown in Fig. 1(h), it is again the intruder $1i_{13/2}$ -state neutrons that mainly contribute the smooth decrease of $\langle r^2 \rangle_\kappa$ up to $A = 208$.

Let us give a little more general discussion on the SO effect around the neutron shell closures. Below the larger magic numbers $N = 50, 82$, and 126, the neutrons filling the intruder $j_>$ state, whose orbital angular momentum is larger than any levels in the shell below, mainly contribute to the decrease of the charge radius as approaching the magic numbers. Above a magic number, the decrease before is eventually compensated by filling of the spin-orbit partner of the intruder, but the other levels may also contribute at the early filling of the new shell. As a result, a local *minimum* of $\langle r^2 \rangle_\kappa$ at or a little beyond $N = 50, 82$, or 126 is developed. It is not the case, however, for the lower magic numbers $N = 8$ and 20 (and $N = 40$) that correspond to the LS closures. In contrast to the $N \geq 50$ shell closures, the single-particle level below (above) an LS closure is $j_<$ ($j_>$), which for the neutron case makes positive (negative) contribution to the charge radius, forming a local *maximum* at $N = 8, 20$, or 40. Such local extrema of $\langle r^2 \rangle_\kappa$ as described above are clearly observed indeed in Fig. 1. This characteristic behavior of $\langle r^2 \rangle_\kappa$ may influence the shape of the isotope shifts, in particular the kink structure as discussed also in Ref. [47]. See also a similar discussion based on the effect of nuclear spin-orbit force in Ref. [15].

B. Comparison with experimental data

Here we compare the following three calculations with experimental data for the charge radius.

1. The RHB calculations are done with $F_{1p}(q^2) = 1$, $F_{1n}(q^2) = 0$, and $F_{2p}(q^2) = F_{2n}(q^2) = 0$, and the charge radius is calculated by $r_{\text{ch}} = \sqrt{\langle r^2 \rangle_p + (0.8 \text{ fm})^2}$, denoted in Figs. 2 and 3 as “+(0.8)²”.
2. The RHB calculations are done with anomalous magnetic moment, i.e., $F_{1p}(q^2) = 1$, $F_{1n}(q^2) = 0$, and $F_{2p}(q^2) = F_{2n}(q^2) = 1$, and the charge radius is calculated by Eq. (8), denoted in Figs. 2 and 3 as “+FF”.
3. Same as 2. but r_{ch} is calculated by Eq. (14) with the CM correction, denoted in Figs. 2 and 3 as “+FF+CM”.

¹ Note that the simple “nonrelativistic approximation” is only a poor approximation to the SO contribution in relativistic mean-field theory, as pointed out in Refs. [46, 50], because of the strong relativistic potentials of hundreds of MeV, but it is still useful to discuss the qualitative behavior of $\langle r^2 \rangle_\kappa$. We have found

indeed that the estimates with Eq. (21), $\langle r^2 \rangle_\kappa$ (fm²) = $-0.0422n$ for ^{4+n}He , = $-0.0211n$ for ^{16+n}O , and = $-0.0127n$ for ^{40}Ca underestimates the RHB results by factor of ≈ 2 in the absolute value but with the correct sign.

1. Absolute values of charge radii

Fig. 2 shows the calculated absolute values of the RMS charge radii r_{ch} in comparison with experimental data. The black dashed lines are the results obtained simply by $r_{\text{ch}} = \sqrt{\langle r^2 \rangle_p + (0.8 \text{ fm})^2}$ without CM and SO corrections, and the green triangles and yellow circles are the ones obtained with only the SO and finite-size correction as in Eq. (8) and with the full correction as in Eq. (14), respectively. The experimental data [1–4] are shown by red squares with error bars.

As was shown also in Sec. III A, both CM and SO influence the charge radii by much more than the experimental uncertainties. The CM correction systematically reduces the charge radii. The effect is most significant for He isotopes, and less for the heavier systems. The SO effect is comparable to the CM correction in light nuclei and dominant in many of heavier nuclei. It is negative except for neutron-deficient C, O, and Ni isotopes and some of the Sn isotopes (see discussion in Sec. III A 2).

The calculated radii with the full correction of the He, C isotopes [Fig. 2(a)], and the Pb isotopes [Fig. 2(d)] tend to near the experimental values, while the agreements in other nuclei are deteriorated by CM and SO corrections. We note again that the fitting of DDME2 parameter set is done for $r_{\text{ch}} = \sqrt{\langle r^2 \rangle_p + (0.8 \text{ fm})^2}$ without CM and SO corrections to ^{16}O , $^{40,48}\text{Ca}$, ^{90}Zr , $^{116,124}\text{Sn}$, and $^{204,208,214}\text{Pb}$ nuclei [51]. It has also to be mentioned that the finite-size effect for “+FF” and “+FF+CM” values of the charge radius are given with different values of the nucleon sizes and the additional $3\kappa\hbar^2/2m^2c^2$ terms as compared to the one adopted in the DDME2 fit [see Eqs. (8) and (14)].

The charge radii of the He isotopes [Fig. 2(a)] are most influenced by the corrections because of small A and Z . Without CM and SO corrections, the charge radius is largest for ^4He and is almost constant along the chain up to ^8He . The slope becomes negative with the SO effect only, but the CM correction makes the slope positive, which follows the trend of the measured charge radii of He isotopes. The large staggering of r_{ch} in ^4He – ^6He – ^8He is not reproduced.

In the C and O isotopes, the CM correction is dominant around $N = Z$, but the SO effect increases as the neutrons fill the $1d_{5/2}$ state while the CM correction becomes smaller. As a result, the total correction is more or less constant along the chains. One sees a kink at ^{24}O due to the SO effect of neutrons filling the $1d_{3/2}$ state.

In the Ni isotopes [Fig. 2(b)], the CM correction dominates over the SO correction for $N \leq 40$. Above $N = 40$, the strong negative SO effects of $1g_{9/2}$ neutrons suppresses the slope of the charge radius, forming a kink at ^{68}Ni which was not observed in the recent measurement [4].

We will discuss the Ca, Ni, Zr, Sn, and Pb isotopes in more detail with the isotope shifts in the next subsection.

2. Isotopic shifts

In order to reduce the systematic error in the calculated values of the charge radius coming from the above mentioned fitting procedure, we show in Fig. 3 the isotopic shifts, defined as the MS charge radius of an isotope A relative to a reference one A' ,

$$\delta \langle r^2 \rangle_{\text{ch}}^{A,A'} = \langle r^2 \rangle_{\text{ch}}(A) - \langle r^2 \rangle_{\text{ch}}(A'). \quad (23)$$

for Ca, Ni, Zr, Sn, and Pb isotopes. Note that the effect of CM correction is also nearly cancelled out by the subtraction for heavier systems.

In Ca isotopes shown in Fig. 3(a), the SO effect of $1f_{7/2}$ neutrons drastically changes the slope of the shift between $A = 40$ and 48. The slight decrease of the charge radius from ^{40}Ca to ^{48}Ca is qualitatively reproduced [48]. It can also be seen that the CM correction slightly decrease the charge radius on $A < 40$ side and increase on the other side, moderating the change of slope beyond $A = 40$. The local maximum of charge radius at ^{44}Ca and the unexpectedly large radius of ^{52}Ca are not reproduced by the present calculations [9, 18].

Fig. 3(b) shows the shifts in the Ni isotopes. A sharp kink at ^{56}Ni observed in a recent experiment [3] is reproduced both with and without the CM and SO corrections. The SO effect sharpens the kink and improves the agree-

ment with the data. Another kink appears at $A = 68$ because of the strong SO effect of $1g_{9/2}$ neutrons. This kink was not observed in another recent experiment [4]. The rapid increase of the measured charge radius above $N = 28$, as in the Ca isotopes, forming an arch-like shape over $N = 28$ –40 is again not reproduced by the present calculations. Note that it was recently pointed out in Ref. [21] that this characteristic behavior of the charge radius between $N = 28$ and 40 is affected by various properties of the mean-field model such as the bulk properties, shell structure, and pairing correlation.

The result for the Zr isotopes is shown in Fig. 3(c). The slope at $A < 90$ region is changed mainly by the SO effect, which improves the agreement with the decrease of the measured charge radius from $A = 88$ to 90 [see also Fig. 1(f)]. The large discrepancy beyond $A = 90$ may be attributed to deformation effect [73].

In Sn isotopes shown in Fig. 3(d), the decline of the slope at $A > 120$ region is well reproduced mainly by the SO effect of $1h_{11/2}$ neutrons, as discussed in the previous subsection. The SO effect above $N = 82$ shell closure is almost flat and smooth due to the scattering of neutrons over the shell above $N = 82$ [see Fig. 1(g)]. This, together with the the SO effect of $1h_{11/2}$ neutrons, leads to a kink at $A = 132$ slightly weaker than is experimentally observed.

Lastly, in Fig. 3(e) showing the Pb isotope chain, the

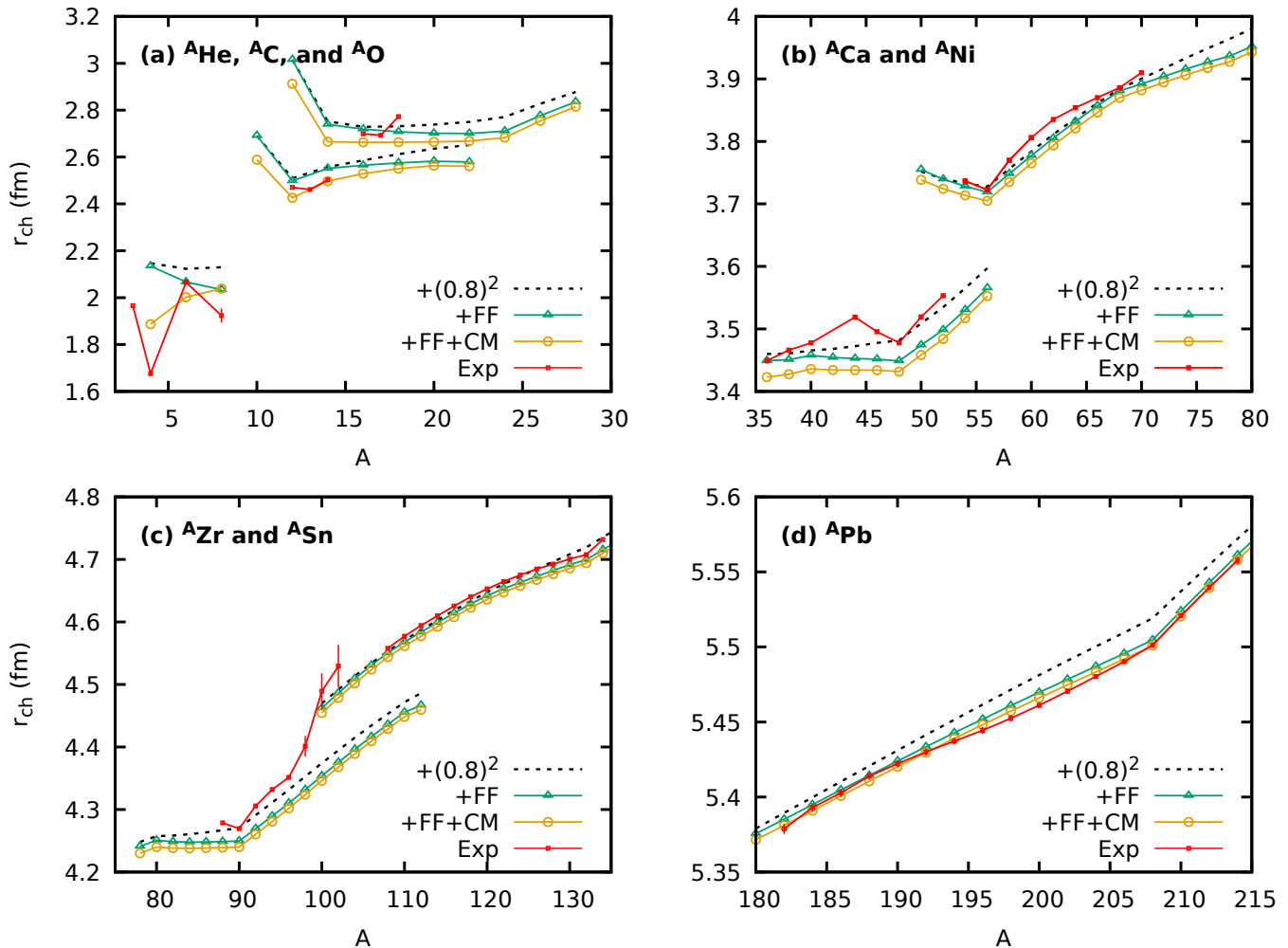


FIG. 2. Comparison to experimental data of the calculated charge radii for (a) He, C, and O isotopes, (b) Ca and Ni isotopes, (c) Zr and Sn isotopes, and (d) Pb isotopes. The dashed lines show the radii calculated by $r_{\text{ch}} = \sqrt{\langle r^2 \rangle_p + (0.8 \text{ fm})^2}$ without CM and SO corrections, the green triangles with only the SO and finite-size corrections as in Eq. (8), and the yellow circles with the full correction as in Eq. (14). The experimental data [1–4] are shown by red squares with error bars.

slope of the $A < 208$ chain is changed by the SO effect of mainly $1i_{13/2}$ neutrons, which yields the constant decrease of the negative SO effect for $A < 208$ [see also Fig. 1(f)]. It improves the region $182 \leq A \leq 192$ but slightly worsen $192 \leq A \leq 206$.

We have also tried the same calculations for DDME δ parameter set [74] and observed qualitatively similar effects of CM and SO corrections, but without a kink at ^{68}Ni . It implies that the SO effect on the kink structure is sensitive to the proton shell structure and the proton occupation probabilities determined by the pairing correlation. See also Ref. [47], in which a number of mean-field models are compared without the CM correction. Global performance studies of the DDME2 and other parameter sets were also done in Refs. [59, 60].

Recently, the effect of the ω - N and ρ - N tensor couplings in a relativistic mean-field model on the charge radii were systematically investigated [17]. It was ob-

served that the impact of the tensor couplings on charge radii is comparable to the effects considered in the present work. The meson-nucleon tensor couplings indirectly influence the charge radius through its effect on the neutron spin-orbit splittings and the neutron occupation probabilities of the single-particle levels [16]. The same effect was also discussed in Ref. [15] with an extra density-dependent nuclear spin-orbit force, which leads to results resembling to ours for the isotope shifts in Ca, Ni, Sn, and Pb chains. On the other hand, the magnetic SO term in the present study, namely the photon-nucleon tensor coupling, is a consequence of the electromagnetic property of the nucleon, which directly modifies the charge density. Note also that the SO effect is entangled with the effect of strong relativistic nuclear mean fields as discussed in Refs. [46, 50] although it is a pure electromagnetic effect, and that the nucleon magnetic moments or more generally the form factors could be modified in nuclear

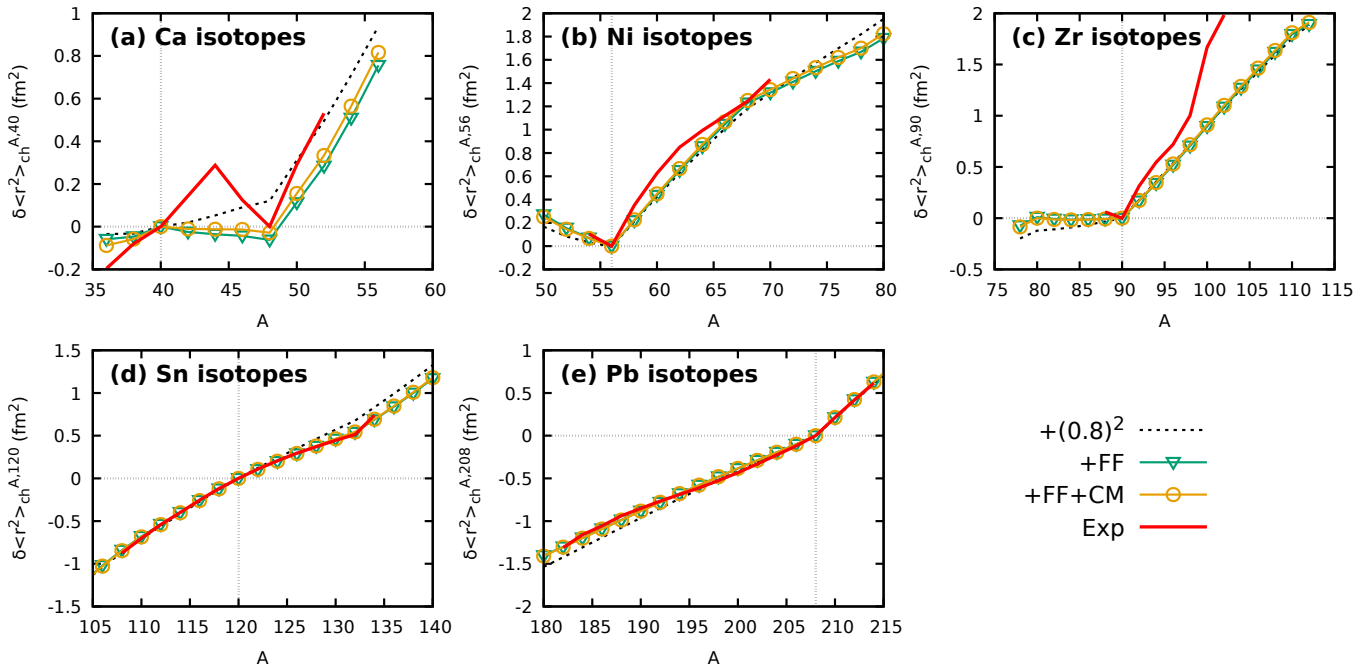


FIG. 3. Calculated isotope shifts compared to the experimental data for (a) Ca, (b) Ni, (c) Zr, (d) Sn, and (e) Pb isotopes. See caption of Fig. 2 for the description of the legends. The experimental data are taken from Ref. [1–4].

medium by the many-body effects and the underlying QCD quark-gluon dynamics [75].

As a final remark, the beyond-mean-field correlations other than the CM correction can also alter the charge radius [20]. The effects of the zeropoint quadrupole-shape fluctuation on charge radius was found to be as large as ~ 0.01 fm [20, 21].

IV. SUMMARY

We have studied the effects of the one- and two-body CM corrections, and the SO term originating from the anomalous magnetic moment of nucleon on the nuclear charge radius. The former is required by the inevitable breaking of translational invariance in the mean-field model, whereas the latter is the electromagnetic property of nucleon affecting directly the nuclear charge-density distribution. The finite-size effects of nucleon from both Dirac and Pauli form factors were also included. We employed an RHB model with DDME2 for ph channel and Gogny D1S for pp channel.

We have observed sizable impacts of each correction on the charge radius from light to heavy nuclei. The light nuclei are significantly affected by the both CM and SO corrections, while the heavier nuclei are much less affected by the former, as expected.

The CM correction consists of one- and two-body parts. The heavier is the system, the more significant is the effect of the two-body part, thus it should not be neglected. We also find that the harmonic-oscillator model

is not a good approximation in light or weakly-bound systems although it is nearly satisfactory for heavy systems.

The magnetic SO effect is more sensitive to the shell structure than the CM correction. In particular, it leads to remarkable improvement of Sn and Pb isotope shifts for DDME2 functional. The SO effect also produces additional kinks at ^{24}O and ^{68}Ni , latter of which is not observed in experimental data.

The two corrections seemingly improve also the agreement with the measured charge radii in very light H and C isotopes. Although the beyond-mean-field correlations are likely to be important in these lighter systems, it was shown that the present mean-field model roughly follows the trend of the measured charge radii.

It would also be interesting to study the effects of the CM correction on the other kinds of radius. More detailed analyses including those of the matter radius and neutron skin thickness will be reported elsewhere.

The CM correction affects also the deformation parameters. The correction of the quadrupole moments can be made in a similar way as the radius since it is quadratic in coordinates. The corrections of higher moments will be much more complicated because there arise three-body and higher operators. However, it is expected that the the CM correction is small for the deformation parameters because cancellation of the correction terms would occur among different spatial directions.

ACKNOWLEDGMENTS

We thank Toshio Suzuki for helpful discussions. We acknowledge support from the Basic Science Research Program of the National Research Foundation of Korea (NRF) under Grants No. 2021R1A6A1A03043957 and No. 2020R1A2C3006177.

Appendix A: Derivation of CM correction on radius

Derivation of Eqs. (3) and (4) is given here. In general, the expectation value of the square of an observable \hat{A} is given by

$$\langle \hat{A}^2 \rangle = \text{Tr}[A^2 \rho] + (\text{Tr}[A \rho])^2 - \text{Tr}[A \rho A \rho] - \text{Tr}[A^* \kappa^* A \kappa], \quad (\text{A1})$$

where ρ and κ are the one-body density matrix and the pairing tensor, respectively, and A is matrix representation of the operator \hat{A} . The first term in the right hand side is the one-body operator part of \hat{A}^2 , while the rest is the two-body part. If \hat{A} is a time-even operator,

$$\langle \hat{A}^2 \rangle = \sum_{\alpha} v_{\alpha}^2 \langle \alpha | A^2 | \alpha \rangle + \left(\sum_{\alpha} v_{\alpha}^2 \langle \alpha | A | \alpha \rangle \right)^2 - \sum_{\alpha\beta} (v_{\alpha}^2 v_{\beta}^2 - u_{\alpha} v_{\alpha} u_{\beta} v_{\beta}) |\langle \alpha | A | \beta \rangle|^2, \quad (\text{A2})$$

where v_{α} and u_{α} are the canonical occupation amplitudes. Note that summations run over the time-reversal partner states pairwise. If \hat{A} is time-odd, on the other hand,

$$\langle \hat{A}^2 \rangle = \sum_{\alpha} v_{\alpha}^2 \langle \alpha | A^2 | \alpha \rangle - \sum_{\alpha\beta} (v_{\alpha}^2 v_{\beta}^2 + u_{\alpha} v_{\alpha} u_{\beta} v_{\beta}) |\langle \alpha | A | \beta \rangle|^2. \quad (\text{A3})$$

Note the opposite signs of the last terms in Eqs. (A2) and (A3). Eq. (A3) applies to the expectation value of the center-of-mass kinetic energy [33].

The proton squared radius with CM correction is given by

$$\begin{aligned} & \left\langle \sum_{i \in p} (\mathbf{r}_i - \mathbf{R}_G)^2 \right\rangle \\ &= Z \langle r^2 \rangle_p - \frac{2}{A} \left\langle \left(\sum_{i \in p} \mathbf{r}_i \right)^2 \right\rangle + \frac{1}{A} \left\langle \left(\sum_{i=1}^A \mathbf{r}_i \right)^2 \right\rangle, \quad (\text{A4}) \end{aligned}$$

where $\mathbf{R}_G = (1/A) \sum_{i=1}^A \mathbf{r}_i$. The second and third terms, which are the CM correction terms, can be computed by (A2) to obtain Eqs. (3) and (4).

Appendix B: Harmonic-oscillator model

In this appendix, we give an analytic estimate, similar to the one in Ref. [37], of the charge radius and the CM correction terms with a harmonic-oscillator (HO) model, and compare them with the experimental data and the RHB results. A connection of our approach with an approximate projection method [32, 41] is also demonstrated at the end.

Let us consider particles with ν intrinsic degrees of freedom (spin and/or isospin) filling HO shells up to the one of \bar{N} quanta. The total number of particles N_p is given by

$$N_p = \sum_{n=0}^{\bar{N}} \nu \frac{1}{2} (n+1)(n+2) = \frac{\nu}{6} (\bar{N}+1)(\bar{N}+2)(\bar{N}+3). \quad (\text{B1})$$

The squared radius within the HO model is given by

$$\begin{aligned} \sum_{\alpha} v_{\alpha}^2 \langle \alpha | r^2 | \alpha \rangle &= \frac{\hbar}{m\omega} \frac{\nu}{8} (\bar{N}+1)(\bar{N}+2)(\bar{N}+3) \\ &= \frac{3}{4} \frac{\hbar}{m\omega} N_p (\bar{N}+2), \quad (\text{B2}) \end{aligned}$$

where $\hbar/m\omega$ is the squared oscillator length which will be determined later. For the CM2 term, we need to compute $\sum_{\alpha\beta} v_{\alpha}^2 v_{\beta}^2 |\langle \alpha | \mathbf{r} | \beta \rangle|^2$. Notice that we neglect the uvv term coming from the pairing tensor since it is only effective near the Fermi surface and much smaller than the $v^2 v^2$ term being a bulk effect. Using the HO matrix element of \mathbf{r} , one obtains

$$\begin{aligned} \sum_{\alpha\beta} v_{\alpha}^2 v_{\beta}^2 |\langle \alpha | \mathbf{r} | \beta \rangle|^2 &= \frac{\nu}{8} \frac{\hbar}{m\omega} \bar{N} (\bar{N}+1)(\bar{N}+2)(\bar{N}+3) \\ &= \frac{3}{4} \frac{\hbar}{m\omega} N_p \bar{N}. \quad (\text{B3}) \end{aligned}$$

The real solution for the algebraic equation (B1) is

$$\bar{N} + 2 = f_{\nu}(N_p)^{1/3} + \frac{1}{3f_{\nu}(N_p)^{1/3}}, \quad (\text{B4})$$

where

$$f_{\nu}(N_p) = \sqrt{\left(\frac{3N_p}{\nu} \right)^2 - \frac{1}{27} + \frac{3N_p}{\nu}}. \quad (\text{B5})$$

It follows from Eqs. (B2), (B3), and (B4) that

$$\sum_{\alpha} v_{\alpha}^2 \langle \alpha | r^2 | \alpha \rangle = \frac{3}{4} \frac{\hbar}{m\omega} N_p \left[f_{\nu}(N_p)^{1/3} + \frac{1}{3} f_{\nu}(N_p)^{-1/3} \right], \quad (\text{B6})$$

and

$$\begin{aligned} & \sum_{\alpha\beta} v_{\alpha}^2 v_{\beta}^2 |\langle \alpha | \mathbf{r} | \beta \rangle|^2 \\ &= \frac{3}{4} \frac{\hbar}{m\omega} N_p \left[f_{\nu}(N_p)^{1/3} + \frac{1}{3} f_{\nu}(N_p)^{-1/3} - 2 \right]. \quad (\text{B7}) \end{aligned}$$

Notice that these two expressions have the same limiting value for $\bar{N} \rightarrow \infty$.

The neutron, proton, and matter MS radii are then given by

$$\langle r^2 \rangle_n = \frac{3}{4} \frac{\hbar}{m\omega_n} \left[f_2(N)^{1/3} + \frac{1}{3} f_2(N)^{-1/3} \right], \quad (\text{B8})$$

$$\langle r^2 \rangle_p = \frac{3}{4} \frac{\hbar}{m\omega_p} \left[f_2(Z)^{1/3} + \frac{1}{3} f_2(Z)^{-1/3} \right], \quad (\text{B9})$$

$$\langle r^2 \rangle_m = \frac{1}{A} (N \langle r^2 \rangle_n + Z \langle r^2 \rangle_p), \quad (\text{B10})$$

respectively. Here we allow the oscillator parameter different between neutron and proton. The CM1 term is given by substituting the above expressions into Eq. (3), and the CM2 term is given as

$$\begin{aligned} \Delta_p^{(\text{CM2})} = & -\frac{3}{4} \frac{\hbar}{m\omega_p} \frac{Z}{A^2} \left(1 - \frac{2A}{Z} \right) \\ & \times \left[f_2(Z)^{1/3} + \frac{1}{3} f_2(Z)^{-1/3} - 2 \right] \\ & - \frac{3}{4} \frac{\hbar}{m\omega_n} \frac{N}{A^2} \\ & \times \left[f_2(N)^{1/3} + \frac{1}{3} f_2(N)^{-1/3} - 2 \right]. \end{aligned} \quad (\text{B11})$$

Note that we treat neutrons and protons separately and do not set $N = Z = A/2$ as is done normally in estimations of this kind [30, 31, 37].

We have made no approximation so far within the HO model. Now we make the only ansatz for the oscillator parameter $\hbar/m\omega$ that remains yet to be determined,

$$\frac{3}{4} \frac{\hbar}{m\omega_n} = \frac{3}{4} \frac{\hbar}{m\omega_p} = \left(\frac{2}{3} \right)^{1/3} \frac{3}{5} r_0^2 A^{1/3}, \quad (\text{B12})$$

with $r_0 \approx 1.2$ fm. This corresponds to approximating the oscillator frequency by $\hbar\omega \approx 41A^{-1/3}$ MeV [30, 31]. One could also consider (N, Z) -dependent oscillators different between neutron and proton, but we take the simplest assumption with a single parameter r_0 . Under this ansatz, the total CM correction simplifies to

$$\Delta_p^{(\text{CM1})} + \Delta_p^{(\text{CM2})} = -\frac{3}{4} \frac{\hbar}{m\omega} \frac{2}{A} \quad (\text{B13})$$

$$= -\left(\frac{2}{3} \right)^{1/3} \frac{6}{5} r_0^2 A^{-2/3}, \quad (\text{B14})$$

which coincides with the expression for the CM correction adopted in TM1 parametrization [36].

In Fig. 4 is shown the the HO-model estimate of the charge radius in comparison with experimental data. The estimate is made by substituting the HO-model values of $\langle r^2 \rangle_p$ and $\Delta_p^{(\text{CM}i)}$ ($i = 1, 2$) into Eq. (14) but without the $\langle r^2 \rangle_n$ and the constant terms. We take $r_0 = 1.23$ fm fitted to the measured charge radii of Pb and Sn isotopes. One can see that the HO model with a single

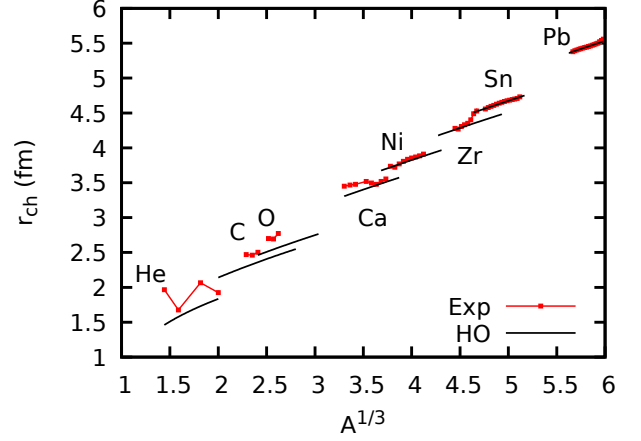


FIG. 4. Charge radii of H, C, O, Ca, Ni, Zr, Sn, and Pb isotopes estimated with the harmonic-oscillator model with $r_0 = 1.23$ fm compared to experimental data. The HO model results and the experimental data are shown by black solid curves and red squares, respectively.

parameter r_0 reproduces the measured charge radii reasonably well from light to heavy nuclei. In particular, the present HO model closely follows the deviation of the measured values from the simple empirical formula $R = r_0 A^{1/3}$. Although the model does not take into account the Coulomb effect, shell effect, deformation, etc., it captures the rough (N, Z) dependence of the radius.

Using the same value of r_0 adjusted to the measured charge radii, we also compare the HO model with RHB results. In Fig. 5, we show the comparison of $\Delta_p^{(\text{CM1})}$ and $\Delta_p^{(\text{CM2})}$ between the RHF calculations and the HO estimates. It is found that the HO model gives only qualitative estimates for H and O isotopes, while the agreement is nearly satisfactory for Ca, Sn, Pb isotopes. There are two reasons of the discrepancies in the light isotopes. First, the enhancement of the radius by the weakly-bound nucleons in near-dripline nuclei is not taken into account in the HO model, as discussed in Sec. III A 1. Second, the simple assumption of $\hbar\omega \approx 41A^{-1/3}$ MeV may not be good for the very light nuclei.

The CM correction for the kinetic energy can also be computed in the HO model as

$$\begin{aligned} \langle \mathbf{P}_{\text{CM}}^2 \rangle & \approx \sum_{\alpha} v_{\alpha}^2 \langle \alpha | p^2 | \alpha \rangle - \sum_{\alpha\beta} v_{\alpha}^2 v_{\beta}^2 |\langle \alpha | \mathbf{p} | \beta \rangle|^2 \\ & = \frac{3}{4} \hbar^2 \frac{m\omega}{\hbar} \cdot 2A. \end{aligned} \quad (\text{B15})$$

From Eqs. (B13) and (B15), one finds the approximate relationship of the CM correction between MS charge radius and kinetic energy,

$$\Delta_p^{(\text{CM1})} + \Delta_p^{(\text{CM2})} = -\frac{9\hbar^2}{4\langle \mathbf{P}_{\text{CM}}^2 \rangle}. \quad (\text{B16})$$

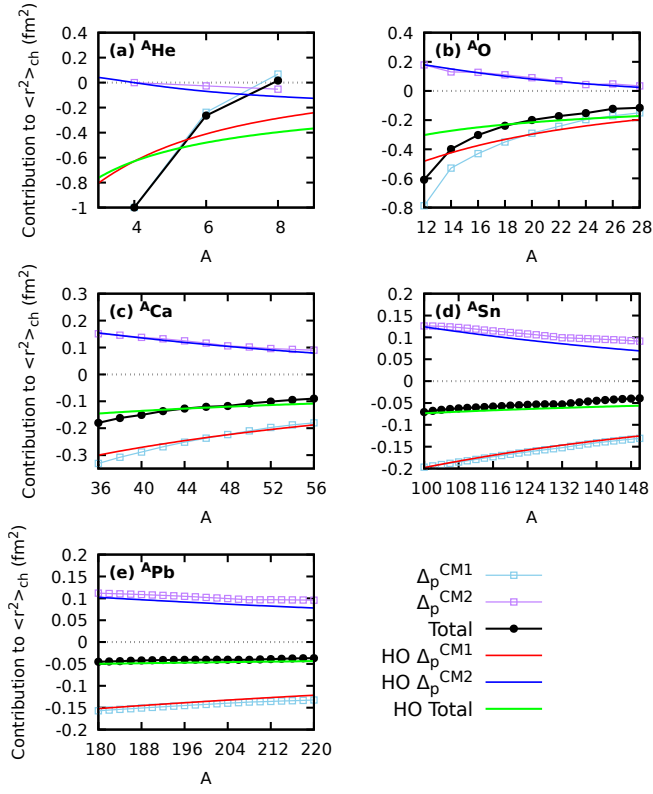


FIG. 5. Comparisons of the CM correction between the HO model ($r_0 = 1.23$ fm) and RHB results for (a) He, (b) O, (c) Ca, (d) Sn, and (e) Pb isotopes. The skyblue and purple squares show the RHB results for one- and two-body CM corrections, respectively, and black dots the total correction $\Delta_p^{(\text{CM1})} + \Delta_p^{(\text{CM2})}$. The HO model estimates for one- and two-body CM correction and their sum are shown by red, blue, and green curves, respectively.

This expression is consistent with the CM correction adopted in Ref. [41] with an approximate projection method [32] giving an additional factor of $\exp\left(\frac{3\hbar^2 q^2}{8(P_{\text{CM}}^2)}\right)$ to the nuclear charge form factor.

-
- [1] I. Angeli and K.P. Marinova, “Table of experimental nuclear ground state charge radii: An update”, *Atomic Data and Nuclear Data Tables* **99**, 69 (2013).
- [2] Tao Li, Yani Luo, and Ning Wang, “Compilation of recent nuclear ground state charge radius measurements and tests for models”, *Atomic Data and Nuclear Data Tables* **140**, 101440 (2013).
- [3] Felix Sommer et al., “Charge Radii of $^{55,56}\text{Ni}$ Reveal a Surprisingly Similar Behavior at $N = 28$ in Ca and Ni Isotopes”, *Phys. Rev. Lett.* **129**, 132501 (2022).
- [4] S. Malbrunot-Ettenauer et al., “Nuclear Charge Radii of the Nickel Isotopes $^{58-68,70}\text{Ni}$ ”, *Phys. Rev. Lett.* **128**, 022502 (2022).
- [5] Skyy V. Pineda, Kristian König, Dominic M. Rossi, B. Alex Brown, Anthony Incorvati, Jeremy Lantis, Kei Minamisono, Wilfried Nörtershäuser, Jorge Piekarewicz, Robert Powel, and Felix Sommer, “Charge Radius of Neutron-Deficient ^{54}Ni and Symmetry Energy Constraints Using the Difference in Mirror Pair Charge Radii”, *Phys. Rev. Lett.* **127**, 182503 (2021).
- [6] T. Kühn, P. Dabkiewicz, C. Duke, H. Fischer, H. -J. Kluge, H. Kremmling, and E. -W. Otten, “Nuclear Shape Staggering in Very Neutron-Deficient Hg Isotopes Detected by Laser Spectroscopy”, *Phys. Rev. Lett.* **39**, 180 (1977).
- [7] M. Anselment, W. Faubel, S. Göring, A. Hanser, G. Meisel, H. Rebel, G. Schatz, “The odd-even staggering of the nuclear charge radii of Pb isotopes”, *Nucl. Phys.* **A451**, 471 (1986).
- [8] B. A. Marsh et al., “Characterization of the shape-staggering effect in mercury nuclei”, *Nat. Phys.* **14**, 1163 (2018).
- [9] A. J. Miller, K. Minamisono, A. Klose, D. Garand, C. Kujawa, J. D. Lantis, Y. Liu, B. Maaß, P. F. Mantica, W. Nazarewicz, W. Nörtershäuser, S. V. Pineda, P.-G. Reinhard, D. M. Rossi, F. Sommer, C. Sumithrarachchi, A. Teigelhöfer, and J. Watkins, “Proton superfluidity and charge radii in proton-rich calcium isotopes”, *Nat. Phys.* **15**, 432 (2019).
- [10] R. P. de Groote et al., “Measurement and microscopic description of odd-even staggering of charge radii of exotic copper isotopes”, *Nat. Phys.* **16**, 620 (2020).
- [11] T. Day Goodacre et al., “Laser Spectroscopy of Neutron-Rich $^{207,208}\text{Hg}$ Isotopes: Illuminating the Kink and Odd-

- Even Staggering in Charge Radii across the $N = 126$ Shell Closure” *Phys. Rev. Lett.* **126**, 032502 (2021).
- [12] Á. Koszorús “Charge radii of exotic potassium isotopes challenge nuclear theory and the magic character of $N = 32$ ”, *Nat. Phys.* **17**, 439 (2021).
- [13] A. Barzakh et al., “Large Shape Staggering in Neutron-Deficient Bi Isotopes” *Phys. Rev. Lett.* **127**, 192501 (2021).
- [14] J. G. Cubiss et al., “Deformation versus Sphericity in the Ground States of the Lightest Gold Isotopes”, *Phys. Rev. Lett.* **131**, 202501 (2023).
- [15] H. Nakada, “Irregularities in nuclear radii at magic numbers”, *Phys. Rev. C* **100**, 044310 (2019).
- [16] U. C. Perera and A. V. Afanasjev, “Differential charge radii: Proton-neutron interaction effects”, *Phys. Rev. C* **107**, 064321 (2023).
- [17] N. Liliani, A.M. Nugraha, J.P. Dinningrum, A. Sulaksono, “Tensor and isovector-isoscalar terms of relativistic mean field model: Impacts on neutron-skin thickness, charge radius, and nuclear matter”, *Nucl. Phys.* **A1042**, 122812 (2024).
- [18] P.-G. Reinhard and W. Nazarewicz, “Toward a global description of nuclear charge radii: Exploring the Fayans energy density functional”, *Phys. Rev. C* **95**, 064328 (2017).
- [19] Myeong-Hwan Mun, Seonghyun Kim, Myung-Ki Cheoun, W.Y. So, Soonchul Choi, and Eunja Ha, “Odd-even shape staggering and kink structure of charge radii of Hg isotopes by the deformed relativistic Hartree-Bogoliubov theory in continuum” *Phys. Lett.* **B847**, 138298 (2023).
- [20] P. Klüpfel, J. Erler, P.-G. Reinhard, and J.A. Maruhn, “Systematics of collective correlation energies from self-consistent mean-field calculations”, *Eur. Phys. J. A* **37**, 343 (2008).
- [21] Markus Kortelainen, Zhonghao Sun, Gaute Hagen, Witold Nazarewicz, Thomas Papenbrock, and Paul-Gerhard Reinhard, “Universal trend of charge radii of even-even Ca-Zn nuclei”, *Phys. Rev. C* **105**, L021303 (2022).
- [22] B. Alex Brown, “Mirror Charge Radii and the Neutron Equation of State”, *Phys. Rev. Lett.* **119**, 122502 (2017).
- [23] B. A. Brown, K. Minamisono, J. Piekarewicz, H. Hergert, D. Garand, A. Klose, K. König, J. D. Lantis, Y. Liu, B. Maaß, A. J. Miller, W. Nörtershäuser, S. V. Pineda, R. C. Powel, D. M. Rossi, F. Sommer, C. Sumithrarachchi, A. Teigelhöfer, J. Watkins, and R. Wirth, “Implications of the ^{36}Ca - ^{36}S and ^{38}Ca - ^{38}Ar difference in mirror charge radii on the neutron matter equation of state”, *Phys. Rev. Research* **2**, 022035(R) (2020).
- [24] Paul-Gerhard Reinhard and Witold Nazarewicz, “Information content of the differences in the charge radii of mirror nuclei”, *Phys. Rev. C* **105**, L021301 (2022).
- [25] Tomoya Naito, Xavier Roca-Maza, Gianluca Colò, Haozhao Liang, and Hiroyuki Sagawa, “Isospin symmetry breaking in the charge radius difference of mirror nuclei”, *Phys. Rev. C* **106**, L061306 (2022).
- [26] Y. N. Huang, Z. Z. Li, and Y. F. Niu, “Correlation between the difference of charge radii in mirror nuclei and the slope parameter of the symmetry energy”, *Phys. Rev. C* **107**, 034319 (2023).
- [27] J. W. Negele, “The mean-field theory of nuclear structure and dynamics”, *Rev. Mod. Phys.* **54**, 913 (1982).
- [28] P.-G. Reinhard, “The relativistic mean-field description of nuclei and nuclear dynamics”, *Rep. Prog. Phys.* **52**, 439 (1989).
- [29] Michael Bender, Paul-Henri Heenen, and Paul-Gerhard Reinhard, “Self-consistent mean-field models for nuclear structure”, *Rev. Mod. Phys.* **75**, 121 (2003).
- [30] P. Ring and P. Schuck, “The Nuclear Many-Body Problems”, (Springer-Verlag Berlin Heidelberg New York, 1980).
- [31] Jean-Paul Blaizot and Georges Ripka, “Quantum Theory of Finite Systems”, (MIT Press, 1986).
- [32] K.W. Schmid, P.-G. Reinhard, “Center-of-mass projection of Skyrme-Hartree-Fock densities”, *Nucl. Phys.* **A530**, 283 (1991).
- [33] M. Bender, K. Rutz, P.-G. Reinhard, and J.A. Maruhn, “Consequences of the center-of-mass correction in nuclear mean-field models”, *Eur. Phys. J. A* **7**, 467 (2000).
- [34] Philippe Da Costa, Karim Bennaceur, Jacques Meyer, Wouter Ryssens, Michael Bender, “On the impact of the scheme for center-of-mass correction on the surface energy of Skyrme Energy Density Functionals”, arXiv:2310.05090 [nucl-th] (2023).
- [35] V. B. Soubbotin, V. I. Tselyaev, and X. Viñas, “Quasiloical density functional theory and its application within the extended Thomas-Fermi approximation”, *Phys. Rev. C* **67**, 014324 (2003).
- [36] Y. Sugahara and H. Toki, “Relativistic mean-field theory for unstable nuclei with non-linear σ and ω terms”, *Nucl. Phys.* **A579**, 557 (1994).
- [37] M.N. Butler, D.W.L. Sprung, and J. Martorell, *Nucl. Phys.* **A422**, 157 (1983).
- [38] Wenhui Long, Jie Meng, Nguyen Van Giai, and Shan-Gui Zhou, “New effective interactions in relativistic mean field theory with nonlinear terms and density-dependent meson-nucleon coupling”, *Phys. Rev. C* **69**, 034319 (2004).
- [39] J. Bartel, P. Quentin, M. Brack, C. Guet, and H.-B. Håkansson, “Towards a better parametrisation of Skyrme-like effective forces: A critical study of the SkM force”, *Nucl. Phys.* **A386**, 79 (1982).
- [40] S. Typel and H.H. Wolter, “Relativistic mean field calculations with density-dependent meson-nucleon coupling”, *Nucl. Phys.* **A656**, 331 (1999).
- [41] Paul-Gerhard Reinhard and Witold Nazarewicz, “Nuclear charge densities in spherical and deformed nuclei: Toward precise calculations of charge radii”, *Phys. Rev. C* **103**, 054310 (2021).
- [42] D. Berdichevsky, R. Fleming, D. W. L. Sprung, and F. Tondeur, “Charge and mass radii of the tin isotopes”, *Z. Phys.* **A329**, 393 (1988).
- [43] Bogdan Mihaila and Jochen H. Heisenberg, “Center-of-mass corrections reexamined: A many-body expansion approach”, *Phys. Rev. C* **60**, 054303 (1999).
- [44] G. Hagen, T. Papenbrock, and D. J. Dean, “Solution of the Center-Of-Mass Problem in Nuclear Structure Calculations”, *Phys. Rev. Lett.* **103**, 062503 (2009).
- [45] C. J. Horowitz and J. Piekarewicz, “Impact of spin-orbit currents on the electroweak skin of neutron-rich nuclei”, *Phys. Rev. C* **86**, 045503 (2012).
- [46] Haruki Kurasawa and Toshio Suzuki, “Effects of the neutron spin-orbit density on the nuclear charge density in relativistic models”, *Phys. Rev. C* **62**, 054303 (2000).
- [47] Tomoya Naito, Tomohiro Oishi, Hiroyuki Sagawa, and Zhiheng Wang, “Comparative study on charge radii and

- their kinks at magic numbers”, *Phys. Rev. C* **107**, 054307 (2023).
- [48] W. Bertozzi, J. Friar, J. Heisenberg and J.W. Negele, “Contributions of neutrons to elastic electron scattering from nuclei”, *Phys. Lett.* **B41**, 408, (1972).
- [49] A. Ong, J. C. Berengut, and V. V. Flambaum, “Effect of spin-orbit nuclear charge density corrections due to the anomalous magnetic moment on halonuclei”, *Phys. Rev. C* **82**, 014320 (2010).
- [50] Haruki Kurasawa and Toshio Suzuki, “The n th-order moment of the nuclear charge density and contribution from the neutrons”, *Prog. Theor. Expt. Phys.* **2019**, 113D01 (2019).
- [51] G. A. Lalazissis, T. Nikšić, D. Vretenar, and P. Ring, “New relativistic mean-field interaction with density-dependent meson-nucleon couplings”, *Phys. Rev. C* **71**, 024312 (2005).
- [52] J.F. Berger, M. Girod and D. Gogny, “Time-dependent quantum collective dynamics applied to nuclear fission”, *Comput. Phys. Comm.* **63**, 365 (1991).
- [53] Walid Younes, Daniel Marc Gogny, and Jean-François Berger, “A Microscopic Theory of Fission Dynamics Based on the Generator Coordinate Method”, (Springer Nature Switzerland AG 2019).
- [54] T. Nikšić, D. Vretenar, P. Finelli, and P. Ring, “Relativistic Hartree-Bogoliubov model with density-dependent meson-nucleon couplings”, *Phys. Rev. C* **66**, 024306 (2002).
- [55] T. Nikšić, N. Paar, D. Vretenar, P. Ring, “DIRHB—A relativistic self-consistent mean-field framework for atomic nuclei”, *Comput. Phys. Comm.* **185**, 1808 (2014).
- [56] G.A. Lalazissis, D. Vretenar, W. Pöschl, P. Ring, “Relativistic Hartree-Bogoliubov description of the neutron drip-line in light nuclei”, *Nucl. Phys.* **A632**, 363 (1998).
- [57] M. Serra and P. Ring, “Relativistic Hartree-Bogoliubov theory for finite nuclei”, *Phys. Rev. C* **65**, 064324 (2002).
- [58] H. Kucharek and P. Ring, “Relativistic field theory of superfluidity in nuclei” *Z. Phys.* **A339**, 23 (1991).
- [59] S. E. Agbemava, A. V. Afanasjev, D. Ray, and P. Ring, “Global performance of covariant energy density functionals: Ground state observables of even-even nuclei and the estimate of theoretical uncertainties”, *Phys. Rev. C* **89**, 054320 (2014).
- [60] U. C. Perera, A. V. Afanasjev, and P. Ring, “Charge radii in covariant density functional theory: A global view”, *Phys. Rev. C* **104**, 064313 (2021).
- [61] Hui Hui Xie and Jian Li, “Impact of Intrinsic Electromagnetic Structure on Nuclear Charge Radius in Relativistic continuum Hartree-Bogoliubov Theory”, arXiv:2308.02309v1 [nucl-th] (2023).
- [62] James J. Kelly, “Nucleon charge and magnetization densities from Sachs form factors”, *Phys. Rev. C* **66**, 065203 (2002).
- [63] J. J. Kelly, “Simple parametrization of nucleon form factors”, *Phys. Rev. C* **70**, 068202 (2004).
- [64] F. J. Ernst, R. G. Sachs, and K. C. Wali, “Electromagnetic Form Factors of the Nucleon”, *Phys. Rev.* **119**, 1105 (1960).
- [65] C.F. Perdrisat, V. Punjabi, and M. Vanderhaeghen, “Nucleon electromagnetic form factors”, *Prog. Part. Nucl. Phys.* **59**, 694 (2007).
- [66] Michael E. Peskin and Daniel V. Schroeder, “An introduction to quantum field theory”, (Perseus Books Publishing L.L.C., 1995).
- [67] T. R. Gentile and C. B. Crawford, “Neutron charge radius and the neutron electric form factor”, *Phys. Rev. C* **83**, 055203 (2011).
- [68] Douglas W. Higinbotham, Al Amin Kabir, Vincent Lin, David Meekins, Blaine Norum, and Brad Sawatzky, “Proton radius from electron scattering data”, *Phys. Rev. C* **93**, 055207 (2016).
- [69] Gerald A. Miller, “Defining the proton radius: A unified treatment”, *Phys. Rev. C* **99**, 035202 (2019).
- [70] Particle Data Group, “Review of Particle Physics”, *Prog. Theor. Expt. Phys.*, **2022**, 083C01 (2022).
- [71] P. Bano, S. P. Pattnaik, M. Centelles, X. Viñas, and T. R. Routray, *Phys. Rev. C* **108**, 015802 (2023).
- [72] D. Vautherin and D. M. Brink, “Hartree-Fock Calculations with Skyrme’s Interaction. I. Spherical Nuclei”, *Phys. Rev. C* **5**, 626 (1972).
- [73] Kaiyuan Zhang et al., “Nuclear mass table in deformed relativistic Hartree-Bogoliubov theory in continuum, I: Even-even nuclei”, *Atomic Data and Nuclear Data Tables* **144**, 101488 (2022).
- [74] X. Roca-Maza, X. Viñas, M. Centelles, P. Ring, and P. Schuck, “Relativistic mean-field interaction with density-dependent meson-nucleon vertices based on microscopical calculations”, *Phys. Rev. C* **84**, 054309 (2011).
- [75] Or Hen, Gerald A. Miller, Eli Piasetzky, and Lawrence B. Weinstein, “Nucleon-nucleon correlations, short-lived excitations, and the quarks within”, *Rev. Mod. Phys.* **89**, 045002 (2017).